

Suppression of current in transport through parallel double quantum dots

Tae-Suk Kim^{1,2} and S. Hershfield²¹*Institute of Physics and Applied Physics, Yonsei University, Seoul 120-749, Korea*²*Department of Physics, University of Florida, Gainesville, Florida 32611-8440*

(Received 1 February 2001; published 8 June 2001)

We report our study of I - V curves in the transport through the quantum dot when an additional quantum dot lying in the Kondo regime is side-connected to it. Due to the Kondo scattering of the effective spin on a side-connected quantum dot, the conductance is suppressed at low temperatures and at low source-drain bias voltages. This zero-bias anomaly is understood as enhanced Kondo scattering with decreasing temperature.

DOI: 10.1103/PhysRevB.63.245326

PACS number(s): 73.21.-b, 72.10.Fk, 72.15.Qm

I. INTRODUCTION

Advances in nanotechnology have made it possible to fabricate quantum dots or artificial atoms and to study their transport properties. Due to the confinement and the Coulomb interaction in the quantum dot, charge and spin can be quantized. Quantization of electron charge leads to the almost periodic variation of conductance as a function of the number of electrons N or the gate voltage. A conductance peak is observed whenever the charge fluctuation is allowed or the N and $(N+1)$ states become energetically degenerate. Otherwise, electrons in the electrodes cannot hop into a quantum dot due to the strong Coulomb repulsion. This Coulomb blockade leads to vanishing conductance between two neighboring conductance peaks. Kondo effects can enhance the conductance in the Coulomb-blockade region when the number of electrons at the quantum dot is odd and at least one electron spin is unpaired. The unpaired $S=\frac{1}{2}$ in the quantum dot can be screened by the electrons in the external electrodes connected to the quantum dot. This theoretical prediction¹ of the nonequilibrium Kondo effects in quantum dot systems was confirmed experimentally recently.²⁻⁴ In the conventional bulk Kondo systems where magnetic ions are doped into normal metals, the study of the Kondo effects was confined to the equilibrium state. In quantum dot systems, the nonequilibrium situation is easily controlled and model parameters can be varied by adjusting the gate voltages.

Study of the Kondo effect in the quantum dot systems has been diversified to see the different aspects. The quantum dots are inserted in the Aharonov-Bohm ring to study the effect of many-body interaction on the persistent current.⁵ When electrons are scattered off the magnetic impurity, they experience a phase shift $\pi/2$ at the Fermi energy due to the Kondo effect. The direct measurement of this phase shift is not possible in the bulk systems. Using a quantum dot inserted into the Aharonov-Bohm ring, the phase shift due to the Kondo effect was studied theoretically⁶ and measured experimentally.⁷ Serial double quantum dots were also studied in the Kondo regime.⁸ Enhanced conductance was observed⁹ in an otherwise Coulomb-blockade region at the spin singlet-to-triplet transition point when the number of electrons on a quantum dot is even. The ground state can be either spin-singlet or spin-triplet depending on the geometry of the confinement potential. Perpendicular magnetic fields can induce a transition of the ground state between spin-

singlet and spin-triplet. These novel Kondo effects have been interpreted as coming from the enhanced Kondo temperature at the transition point.¹⁰

In this paper, we study theoretically the transport properties of parallel double quantum dots as depicted in Fig. 1. One *active* quantum dot is connected to the source and drain electrodes and the other quantum dot is *side-connected* to the active quantum dot. Since the energy levels in two quantum dots can be controlled separately using the gate voltage, different transport regimes can be probed. In this work, we present our study of the I - V characteristics of this system when the active quantum dot lies in the conductance peak region while the side-connected quantum dot lies in the Coulomb-blockade region. In this case, charge fluctuations are suppressed and an effective spin $S=\frac{1}{2}$ arises in a side-connected dot. Electrons passing through the active dot experience the Kondo scattering off an effective spin in a side-connected dot. We find that the linear-response conductance is suppressed at low temperature due to the enhanced Kondo scattering off spin $S=\frac{1}{2}$. The spectral function at a side-connected dot develops a Kondo resonance peak as the temperature is lowered. On the other hand, the spectral function at the active dot becomes depleted near $\omega=0$ with decreasing temperature. We obtained these results using the nonequilibrium Green's function method combined with the noncrossing approximation (NCA).

This paper is organized as follows. In Sec. II, we introduce our model Hamiltonian and present the formulation of current passing through an active dot. The relevant Green's

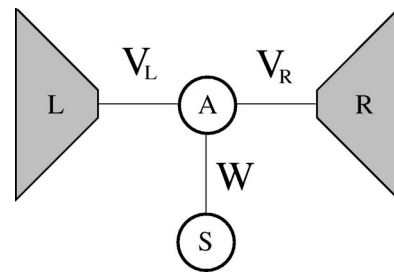


FIG. 1. Schematic display of parallel double quantum dots. The *active* quantum dot A is connected to two left and right electrodes and the other dot S is *side-connected* to the dot A . A side-connected dot S provides an additional current path or acts as a scattering center of electrons passing through the dot A .

functions in nonequilibrium are formulated in Sec. III using the NCA, which is modified for our system. Numerical results, solving the NCA equations self-consistently, are presented in Sec. IV and a conclusion is included in Sec. V.

II. PARALLEL DOUBLE QUANTUM DOTS

A. Model Hamiltonian

Consider the parallel double quantum dots shown in Fig. 1. In this experimental geometry, the transfer of electrons from one electrode to the other is realized by hopping on and off an *active* quantum dot (the site A). The other dot (the site S) is *side-connected* to the active dot by hopping. Assuming that the energy-level spacing is large enough compared to the level broadening due to the tunneling into two electrodes, the model Hamiltonian can be written as

$$H = H_{\text{el}} + H_{\text{qdot}} + H_1, \quad (2.1a)$$

$$H_{\text{el}} = \sum_{p=L,R} \sum_{\vec{k}\alpha} \epsilon_{p\vec{k}} c_{p\vec{k}\alpha}^\dagger c_{p\vec{k}\alpha}, \quad (2.1b)$$

$$H_{\text{qdot}} = \sum_{i=A,S} \sum_{\alpha} E_i d_{i\alpha}^\dagger d_{i\alpha} + \sum_{i=A,S} U_i n_{i\uparrow} n_{i\downarrow}, \quad (2.1c)$$

$$H_1 = \sum_{p=L,R} \sum_{\vec{k}\alpha} [V_p(\vec{k}) c_{p\vec{k}\alpha}^\dagger d_{A\alpha} + V_p^*(\vec{k}) d_{A\alpha}^\dagger c_{p\vec{k}\alpha}] + \sum_{\alpha} [W d_{A\alpha}^\dagger d_{S\alpha} + W^* d_{S\alpha}^\dagger d_{A\alpha}]. \quad (2.1d)$$

The electron creation operator of spin α in the electrode $p = L, R$ is $c_{p\vec{k}\alpha}^\dagger$. The index $p = L$ (R) denotes the left (right) external electrode. Both electrodes are assumed to be described by the Lorentzian density of states (DOS) with the energy dispersion $\epsilon_{p\vec{k}} \equiv \epsilon_{\vec{k}} + \mu_p$. $\mu_{L,R} = \pm \frac{1}{2} eV$ is the chemical potential shift due to the bias voltage applied to the electrodes. $d_{i\alpha}^\dagger$ is the electron creation operator in a quantum dot $i = A, S$ with A (S) labeling an active (side-connected) dot, respectively. U_i is the on-site electron-electron Coulomb interaction in a dot i .

When $U_A = U_S = 0$, two dots become resonant levels and the solution can be found analytically (see Appendix A). The model becomes nontrivial when one of the on-site Coulomb interactions or both are nonzero. In this paper, we are going to study the case of $U_A = 0$ and $U_S \neq 0$ in detail. When U_S is the largest of all the model parameters and $-E_S \gg |W|$, charge fluctuations in a side-connected dot can be neglected and the side-connected dot can be treated as an effective spin $S = \frac{1}{2}$. In this case, removing the charge degrees of freedom in a side-connected dot (Schrieffer-Wolf transformation¹¹), the interaction between two dots can be derived,

$$H_{AS} = J_{AS} \vec{S}_S \cdot \sum_{\alpha\beta} d_{A\alpha}^\dagger \frac{1}{2} \vec{\sigma}_{\alpha\beta} d_{A\beta}, \quad J_{AS} = \frac{2|W|^2}{-E_S} + \frac{2|W|^2}{U_S + E_S}. \quad (2.2)$$

Here $\vec{S}_S = \sum_{\alpha\beta} |S; \alpha\rangle \frac{1}{2} \vec{\sigma}_{\alpha\beta} \langle S; \beta|$ represents the spin degrees of freedom in a side-connected dot in the absence of charge fluctuations. Electrons, flowing from the left electrode to the right, at the active dot will experience the Kondo scattering off an effective spin of a side-connected dot. Appendix B contains the details of the $U_A \neq 0$ and $U_S \neq 0$ case.

B. Formulation of current

The current operator can be defined as a variation of the number operators of electrons per unit time leaving one electrode ($p = L, R$),

$$\begin{aligned} \hat{I}_p &\equiv -e(-\dot{N}_p) \\ &= \frac{e}{i\hbar} [N_p, H] \\ &= \frac{e}{i\hbar} \sum_{\vec{k}\alpha} [V_p(\vec{k}) c_{p\vec{k}\alpha}^\dagger d_{A\alpha} - \text{H.c.}]. \end{aligned} \quad (2.3)$$

The measured current is given by the thermal average of the above current operator and can be written in terms of the lesser Green's functions out of equilibrium,¹²

$$I_p(t) = -ie \sum_{\vec{k}\alpha} [V_p(\vec{k}) G_{Acp}^<(\vec{k}; t, t) - V_p^*(\vec{k}) G_{cpA}^<(\vec{k}; t, t)]. \quad (2.4)$$

The current can be expressed in terms of Green's functions for the conduction electrons and quantum dots using the Dyson equations for the mixed Green's functions,

$$\begin{aligned} G_{cpA}(\vec{k}; t, t') &\equiv \frac{1}{i\hbar} \langle T c_{p\vec{k}\alpha}(t) d_{A\alpha}^\dagger(t') \rangle \\ &= V_p(\vec{k}) \int_C dt_1 G_{cp}(\vec{k}; t, t_1) D_A(t_1, t'), \end{aligned} \quad (2.5a)$$

$$\begin{aligned} G_{Acp}(\vec{k}; t, t') &\equiv \frac{1}{i\hbar} \langle T d_{A\alpha}(t) c_{p\vec{k}\alpha}^\dagger(t') \rangle \\ &= V_p^*(\vec{k}) \int_C dt_1 D_A(t, t_1) G_{cp}(\vec{k}; t_1, t'), \end{aligned} \quad (2.5b)$$

$$i\hbar D_i(t, t') = \langle T d_{i\alpha}(t) d_{i\alpha}^\dagger(t') \rangle, \quad i = A, S. \quad (2.5c)$$

Here the subscript C in the time-integral means the Keldysh contour. Using analytic continuation to the real-time axis,¹³ we can find the lesser part of $G_{Acp}(\vec{k}; t, t')$,

$$\begin{aligned} G_{Acp}^<(\vec{k}; t, t') &= V_p^*(\vec{k}) \int dt_1 [D_A^<(t, t_1) G_{cp}^a(\vec{k}; t_1, t') \\ &\quad + D_A^r(t, t_1) G_{cp}^<(\vec{k}; t_1, t')]. \end{aligned} \quad (2.6)$$

The current can be expressed as

$$\begin{aligned}
 I_p &= -ie \frac{1}{V} \sum_{\vec{k}\alpha} |V_p(\vec{k})|^2 \int \frac{d\omega}{2\pi} \{D_A^<(\omega) [\Sigma_{cp}^a(\omega) - \Sigma_{cp}^r(\omega)] \\
 &\quad + \Sigma_{cp}^<(\omega) [D_A^r(\omega) - D_A^a(\omega)]\} \\
 &= -ie \sum_{\alpha} \int \frac{d\omega}{2\pi} |D_A^r(\omega)|^2 \{ \Sigma_A^<(\omega) [\Sigma_{cp}^a(\omega) - \Sigma_{cp}^r(\omega)] \\
 &\quad + \Sigma_{cp}^<(\omega) [\Sigma_A^r(\omega) - \Sigma_A^a(\omega)] \}. \quad (2.7)
 \end{aligned}$$

Here Σ_A is the self-energy for the active dot A and the following equations are used:

$$\Sigma_{cp}(t, t') = \frac{1}{V} \sum_{\vec{k}} |V_p(\vec{k})|^2 G_{cp}(\vec{k}; t, t'), \quad (2.8a)$$

$$\Sigma_{cp}^{r,a}(\omega) = \int \frac{d\epsilon}{\pi} \frac{\Gamma_p(\epsilon)}{\hbar\omega - \epsilon \pm i\delta}, \quad (2.8b)$$

$$\Sigma_{cp}^{<, >}(\omega) = 2\Gamma_p(\omega) f_p(\pm\omega), \quad (2.8c)$$

$$\Gamma_p(\omega) \equiv \frac{\pi}{V} \sum_{\vec{k}} |V_p(\vec{k})|^2 \delta(\hbar\omega - \epsilon_{p\vec{k}}). \quad (2.8d)$$

The above equation for the current is quite general and can be used as a starting point in reducing the expression of current in specific cases.

The average number of electrons at a side-connected dot S should remain the same in a steady state. This condition is essential to get the right expression for the current flowing from the left to the right electrodes. That is, the net current flowing out of the dot S should vanish for

$$\begin{aligned}
 I_S &= \frac{e}{i\hbar} \sum_{\alpha} [W^* \langle d_{S\alpha}^{\dagger} d_{A\alpha} \rangle - W \langle d_{A\alpha}^{\dagger} d_{S\alpha} \rangle] \\
 &= -ie \sum_{\alpha} [W^* G_{AS}^<(t, t) - W G_{SA}^<(t, t)]. \quad (2.9)
 \end{aligned}$$

The current I_S was expressed in terms of the mixed Green's functions,

$$i\hbar G_{AS}(t, t') = \langle T d_{A\alpha}(t) d_{S\alpha}^{\dagger}(t') \rangle, \quad (2.10a)$$

$$i\hbar G_{SA}(t, t') = \langle T d_{S\alpha}(t) d_{A\alpha}^{\dagger}(t') \rangle. \quad (2.10b)$$

These mixed Green's functions can be written as

$$\begin{aligned}
 G_{AS}(t, t') &= W \int_C dt_1 \tilde{D}_A(t, t_1) D_S(t_1, t') \\
 &= W \int_C dt_1 D_A(t, t_1) \tilde{D}_S(t_1, t'), \quad (2.11a)
 \end{aligned}$$

$$\begin{aligned}
 G_{SA}(t, t') &= W^* \int_C dt_1 \tilde{D}_S(t, t_1) D_A(t_1, t') \\
 &= W^* \int_C dt_1 D_S(t, t_1) \tilde{D}_A(t_1, t'). \quad (2.11b)
 \end{aligned}$$

Here D_A and D_S are the fully dressed Green's functions of the dots A and S , respectively,

$$i\hbar D_A(t, t') = \langle T d_{A\alpha}(t) d_{A\alpha}^{\dagger}(t') \rangle, \quad (2.12a)$$

$$i\hbar D_S(t, t') = \langle T d_{S\alpha}(t) d_{S\alpha}^{\dagger}(t') \rangle. \quad (2.12b)$$

On the other hand, \tilde{D}_A and \tilde{D}_S are the corresponding Green's functions, which cannot be separated into two parts by removing one tunneling matrix W . Using analytic continuation, the current I_S can be written as

$$\begin{aligned}
 I_S &= -ie |W|^2 \sum_{\alpha} \int \frac{d\omega}{2\pi} \{ [\tilde{D}_A^r(\omega) - \tilde{D}_A^a(\omega)] D_S^<(\omega) \\
 &\quad - [D_S^r(\omega) - D_S^a(\omega)] \tilde{D}_A^<(\omega) \} \\
 &= e \sum_{\alpha} \int \frac{d\omega}{2\pi} 2|W|^2 |\tilde{D}_A^r(\omega)|^2 [\pi \tilde{\Sigma}_A^<(\omega) A_S(\omega) \\
 &\quad + \text{Im}\{\tilde{\Sigma}_A^r(\omega)\} D_S^<(\omega)]. \quad (2.13)
 \end{aligned}$$

Since $I_S=0$ in steady state, we find the equation relating the lesser part to the retarded part of the Green's function or the spectral function A_S for the dot S ,

$$D_S^<(\omega) = \pi \frac{\tilde{\Sigma}_A^<(\omega)}{-\text{Im}\tilde{\Sigma}_A^r(\omega)} A_S(\omega), \quad (2.14a)$$

$$f_{\text{eff}}(\omega) = \frac{\tilde{\Sigma}_A^<(\omega)}{-2\text{Im}\tilde{\Sigma}_A^r(\omega)}. \quad (2.14b)$$

That is, the condition that no net current flows out of the dot S determines its nonequilibrium thermal distribution function. The current I_S can be expressed in another form,

$$\begin{aligned}
 I_S &= -ie |W|^2 \sum_{\alpha} \int \frac{d\omega}{2\pi} \{ [D_A^r(\omega) - D_A^a(\omega)] \tilde{D}_S^<(\omega) \\
 &\quad - [\tilde{D}_S^r(\omega) - \tilde{D}_S^a(\omega)] D_A^<(\omega) \} \\
 &= e \sum_{\alpha} \int \frac{d\omega}{2\pi} 2|W|^2 |D_A^r(\omega)|^2 \\
 &\quad \times [\pi \Sigma_A^<(\omega) \tilde{A}_S(\omega) + \text{Im}\{\Sigma_A^r(\omega)\} \tilde{D}_S^<(\omega)]. \quad (2.15)
 \end{aligned}$$

C. Interacting case: $U_A=0$ and $U_S \neq 0$

When $U_A=0$ and $U_S \neq 0$, the active dot A becomes a resonant level and the side-connected dot S is strongly correlated. This model Hamiltonian may describe the situation that the dot A lies in the conductance peak region and the dot S in the Kondo or Coulomb-blockade region. Green's functions of the two dots are given by the Dyson equations with the self-energies being given by

$$\Sigma_A(t, t') = \Sigma_c(t, t') + W^2 \tilde{D}_S(t, t'), \quad (2.16a)$$

$$\Sigma_S(t, t') = \Sigma_U(t, t') + W^2 \tilde{D}_A(t, t'). \quad (2.16b)$$

Here $\Sigma_c(t, t') = \Sigma_{cL}(t, t') + \Sigma_{cR}(t, t')$ [Eq. (2.8a)] is the self-energy coming from tunneling into left and right electrodes, $\Sigma_U(t, t')$ is the self-energy for a dot S due to the on-site Coulomb interaction, and the auxiliary Green's functions are defined by the Dyson equations

$$\begin{aligned} \tilde{D}_A(t, t') &= D_{A0}(t, t') + \int_C dt_1 \int_C dt_2 \tilde{D}_A(t, t_1) \\ &\quad \times \Sigma_c(t_1, t_2) D_{A0}(t_2, t'), \end{aligned} \quad (2.17a)$$

$$\begin{aligned} \tilde{D}_S(t, t') &= D_{S0}(t, t') + \int_C dt_1 \int_C dt_2 \tilde{D}_S(t, t_1) \\ &\quad \times \Sigma_U(t_1, t_2) D_{S0}(t_2, t'). \end{aligned} \quad (2.17b)$$

From the self-energy equations, we find

$$\Sigma_A^<(\omega) = 2\Gamma_L(\omega)f_L(\omega) + 2\Gamma_R(\omega)f_R(\omega) + W^2\tilde{D}_S^<(\omega), \quad (2.18a)$$

$$\begin{aligned} \Sigma_A^r(\omega) - \Sigma_A^a(\omega) &= -2i[\Gamma_L(\omega) + \Gamma_R(\omega)] \\ &\quad + |W|^2[\tilde{D}_S^r(\omega) - \tilde{D}_S^a(\omega)]. \end{aligned} \quad (2.18b)$$

Inserting all the equations into the expression of the current (2.7), we find

$$\begin{aligned} I_p &= e \sum_{\alpha} \int \frac{d\omega}{2\pi} \{4\Gamma_L(\omega)\Gamma_R(\omega)|D^r(\omega)|^2[f_p^-(\omega) - f_p(\omega)] \\ &\quad + 2|W|^2\Gamma_p(\omega)|D_A^r(\omega)|^2[\tilde{D}_S^<(\omega) - 2\pi f_p(\omega)\tilde{A}_S(\omega)]\}. \end{aligned} \quad (2.19)$$

From the condition $I_S = 0$, we have

$$\begin{aligned} \tilde{D}_S^<(\omega) &= \pi \frac{\Sigma_A^<(\omega)}{-\text{Im}\Sigma_A^r(\omega)} \tilde{A}_S(\omega) \\ &= \frac{2\pi[\Gamma_L(\omega)f_L(\omega) + \Gamma_R(\omega)f_R(\omega)] + \pi|W|^2\tilde{A}_S^<(\omega)}{\Gamma_L(\omega) + \Gamma_R(\omega) + \pi|W|^2\tilde{A}_S(\omega)} \\ &\quad \times \tilde{A}_S(\omega) \\ &= 2\pi f_{\text{eff}}(\omega)\tilde{A}_S(\omega), \end{aligned} \quad (2.20a)$$

$$f_{\text{eff}}(\omega) \equiv \frac{\Gamma_L(\omega)f_L(\omega) + \Gamma_R(\omega)f_R(\omega)}{\Gamma_L(\omega) + \Gamma_R(\omega)}. \quad (2.20b)$$

It follows from the relation $I_S = 0$ that $D_S^<(\omega) = 2\pi f_{\text{eff}}(\omega)\tilde{A}_S(\omega)$. The effective Fermi-Dirac function $f_{\text{eff}}(\omega)$ describes the nonequilibrium thermal distribution at the dot S and also at the active dot A . [It can be shown from Eq. (2.22).] The current flowing from the left to the right electrode becomes

$$I_L = e \sum_{\alpha} \int \frac{d\omega}{2\pi} T(\omega)[f_R(\omega) - f_L(\omega)], \quad (2.21a)$$

$$\begin{aligned} T(\omega) &= 4\Gamma_L(\omega)\Gamma_R(\omega)|D_A^r(\omega)|^2 \left[1 + \frac{\pi|W|^2\tilde{A}_S(\omega)}{\Gamma_L(\omega) + \Gamma_R(\omega)} \right] \\ &= \frac{4\pi\Gamma_L(\omega)\Gamma_R(\omega)}{\Gamma_L(\omega) + \Gamma_R(\omega)} A_A(\omega). \end{aligned} \quad (2.21b)$$

Note that the current I_L consists of two contributions, coming from the direct path ($L \rightarrow A \rightarrow R$) and the indirect path ($L \rightarrow A \rightarrow S \rightarrow A \rightarrow R$), which are interfering with each other.

The current is written down in terms of the transmission coefficient, that is, in Landauer-Büttiker form. In turn, the transmission coefficient is proportional to the spectral function of the active dot A . To find the spectral function $A_A(\omega)$, we note that Green's functions of the two dots are related to each other by the equations

$$D_A^r(\omega) = \tilde{D}_A^r(\omega) + |W|^2\tilde{D}_A^r(\omega)D_S^r(\omega)\tilde{D}_A^r(\omega). \quad (2.22)$$

To get the desired spectral function, we have to calculate the Green's function D_S^r at a side-connected dot and the auxiliary Green's function \tilde{D}_A^r at the active dot is given by Eq. (2.17a). Due to the on-site Coulomb interaction at a side-connected dot S , the calculation of $D_S^r(\omega)$ is highly nontrivial and requires a many-body calculation. In the next section, we describe the noncrossing approximation in order to find the Green's function at a side-connected dot S .

III. NONCROSSING APPROXIMATION (NCA)

To study the I - V curves of our model system, we need to calculate the Green's function at a side-connected dot S out of equilibrium. For this purpose, we adopt the NCA, which has been a very fruitful tool for the study of the Anderson model in both equilibrium^{14,15} and nonequilibrium.^{16,17}

To begin with, we need to identify the effective continuum band for the dot S . In the Anderson model, which describes the magnetic ions imbedded in normal metals, the self-energy can be written as a sum of two contributions,

$$\Sigma_f(\omega) = \int \frac{d\epsilon}{\pi} \frac{\Gamma_{\text{eff}}(\epsilon)}{\hbar\omega - \epsilon + i\delta} + \Sigma_U^r(\omega). \quad (3.1)$$

The first term is the one-body contribution from tunneling into the conduction band and the second term Σ_U is the many-body contribution from the on-site Coulomb interaction. On the other hand, the self-energy of the dot S in our model is given by

$$\Sigma_S(\omega) = |W|^2\tilde{D}_A^r(\omega) + \Sigma_U^r(\omega). \quad (3.2)$$

Comparing the two self-energies [Eqs. (3.1) and (3.2)], we can identify that the effective Anderson hybridization function is given by the equation

$$\begin{aligned} \Gamma_{\text{eff}}(\epsilon) &= -|W|^2 \text{Im}\tilde{D}_A^r(\epsilon) \\ &= -|W|^2 \text{Im} \left\{ \frac{1}{\epsilon - E_d - \Sigma_c^r(\epsilon)} \right\} \\ &= \pi|W|^2\tilde{A}_A(\epsilon). \end{aligned} \quad (3.3)$$

The effective continuum band for the dot S is represented by the auxiliary Green's function $\tilde{D}_A(t, t')$.

To find the Green's function for the dot S , we do a perturbative expansion in W . To begin with, we represent the Fock space of the dot S by the pseudoparticle operators. In the large U_S limit, we may neglect the double occupation,

$$d_{S\alpha} \rightarrow b^\dagger f_\alpha. \quad (3.4)$$

The boson operator b annihilates the empty state and the pseudofermion operator f_α destroys the singly occupied state at the dot S . After replacing the electron operator $d_{S\alpha}$ by the pseudoparticle operators, the occupation constraint has to be enforced: $Q=1$,

$$Q = \sum_\alpha f_\alpha^\dagger f_\alpha + b^\dagger b. \quad (3.5)$$

This constraint is taken into account using the Lagrange multiplier method: $H \rightarrow H + \lambda(Q-1)$. The projection to the physical Hilbert space $Q=1$ leads to the following projection rule for the physical observables:

$$O(\omega) = \frac{1}{Z_S} \lim_{\lambda \rightarrow \infty} e^{\beta\lambda} O_\lambda(\omega \rightarrow \omega + \lambda), \quad (3.6)$$

$$Z_S = \lim_{\lambda \rightarrow \infty} e^{\beta\lambda} \langle Q \rangle_\lambda. \quad (3.7)$$

Here $O_\lambda(\omega)$ is a thermal average of observable operator \hat{O} for the Hamiltonian $H + \lambda(Q-1)$. The Feynman diagram rules for the Green's functions are very simple. In the $2n$ th order, there are $3n+1$ pairs of creation and annihilation operators. This leads to the factor $[i\hbar]^{-2n}[i\hbar]^{3n+1}$. Canceling one factor $i\hbar$ leads to the following factor: $(-1)^{N_F}[i\hbar]^n|W|^{2n}$, where N_F is the number of closed fermion loops. With this rule, the NCA self-energies (displayed in Fig. 2) are given by the equations

$$\Sigma_f(\lambda; t, t') = i\hbar|W|^2 G_b(\lambda; t, t') \tilde{D}_A(t, t'), \quad (3.8a)$$

$$\Sigma_b(\lambda; t, t') = -i\hbar N_s |W|^2 G_f(\lambda; t, t') \tilde{D}_A(t', t). \quad (3.8b)$$

Here $N_s=2$ accounts for the spin degeneracy of the singly occupied state for the dot S . G_b and G_f are the pseudoparticle Green's functions of boson and fermion, respectively. Using an analytic continuation to the real-time axis,¹³ we find

$$\Sigma_f^>(\lambda; t, t') = |W|^2 G_b^>(\lambda; t, t') \tilde{D}_A^>(t, t'), \quad (3.9a)$$

$$\Sigma_f^<(\lambda; t, t') = -|W|^2 G_b^<(\lambda; t, t') \tilde{D}_A^<(t, t'), \quad (3.9b)$$

$$\begin{aligned} \Sigma_f^r(\lambda; t, t') = & |W|^2 [G_b^r(\lambda; t, t') \tilde{D}_A^>(t, t') \\ & - G_b^<(\lambda; t, t') \tilde{D}_A^r(t, t')], \end{aligned} \quad (3.9c)$$

$$\Sigma_b^>(\lambda; t, t') = N_s |W|^2 G_f^>(\lambda; t, t') \tilde{D}_A^<(t', t), \quad (3.9d)$$

$$\Sigma_b^<(\lambda; t, t') = -N_s |W|^2 G_f^<(\lambda; t, t') \tilde{D}_A^>(t', t), \quad (3.9e)$$

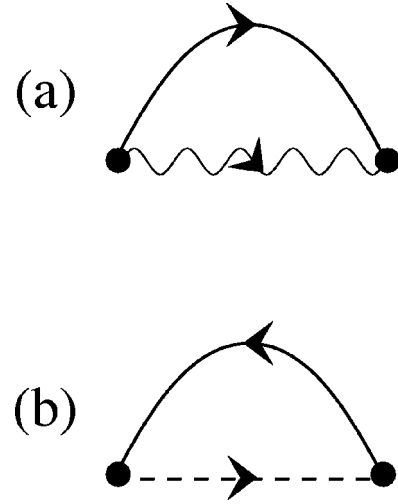


FIG. 2. NCA self-energy diagrams for (a) pseudofermion and (b) slave boson. The solid line represents the propagator \tilde{D} , the Green's function of the active dot A when $W=0$. The dashed (wavy) line is the pseudofermion (boson) propagator. The solid circle means the tunneling matrix W .

$$\begin{aligned} \Sigma_b^r(\lambda; t, t') = & N_s |W|^2 [G_f^r(\lambda; t, t') \tilde{D}_A^<(t', t) \\ & + G_f^<(\lambda; t, t') \tilde{D}_A^r(t', t)]. \end{aligned} \quad (3.9f)$$

To give a concrete example of analytic continuation, we consider the derivation of $\Sigma_b^>(\lambda; t, t')$:

$$\frac{1}{i} \Sigma_b^>(\lambda; t, t') = -i\hbar |W|^2 \frac{1}{i} G_f^>(\lambda; t, t') \times \frac{-1}{i} \tilde{D}_A^<(t', t). \quad (3.10)$$

Removing the common factors on both sides of the equation, we find the desired expression for $\Sigma_b^>(\lambda; t, t')$.

After Fourier transform, we get the self-energy equations

$$\Sigma_f^>(\lambda; \omega) = |W|^2 \int \frac{d\xi}{2\pi} G_b^>(\lambda; \omega - \xi) \tilde{D}_A^>(\xi), \quad (3.11a)$$

$$\Sigma_f^<(\lambda; \omega) = -|W|^2 \int \frac{d\xi}{2\pi} G_b^<(\lambda; \omega - \xi) \tilde{D}_A^<(\xi), \quad (3.11b)$$

$$\begin{aligned} \Sigma_f^r(\lambda; \omega) = & |W|^2 \int \frac{d\xi}{2\pi} [G_b^r(\lambda; \omega - \xi) \tilde{D}_A^>(\xi) \\ & - G_b^<(\lambda; \omega - \xi) \tilde{D}_A^r(\xi)], \end{aligned} \quad (3.11c)$$

$$\Sigma_b^>(\lambda; \omega) = N_s |W|^2 \int \frac{d\xi}{2\pi} G_f^>(\lambda; \omega + \xi) \tilde{D}_A^<(\xi), \quad (3.11d)$$

$$\Sigma_b^<(\lambda; \omega) = -N_s |W|^2 \int \frac{d\xi}{2\pi} G_f^<(\lambda; \omega + \xi) \tilde{D}_A^>(\xi), \quad (3.11e)$$

$$\begin{aligned} \Sigma_b^r(\lambda; \omega) = & N_s |W|^2 \int \frac{d\zeta}{2\pi} [G_f^r(\lambda; \omega + \zeta) \tilde{D}_A^<(\zeta) \\ & + G_f^<(\lambda; \omega + \zeta) \tilde{D}_A^a(\zeta)]. \end{aligned} \quad (3.11f)$$

The Green's function at the dot S can be written down in terms of pseudoparticle operators,

$$\begin{aligned} i\hbar D_S(\lambda; t, t') = & \langle T d_{S\alpha}(t) d_{S\alpha}^\dagger(t') \rangle \\ = & \langle T b^\dagger(t) f_\alpha(t) f_\alpha^\dagger(t') b(t') \rangle. \end{aligned} \quad (3.12)$$

In the leading approximation, the desired Green's function is

$$D_S(\lambda; t, t') \approx i\hbar G_f(\lambda; t, t') G_b(\lambda; t', t). \quad (3.13)$$

Analytic continuation to the real-time axis¹³ leads to

$$D_S^>(\lambda; t, t') = -G_f^>(\lambda; t, t') G_b^<(\lambda; t', t), \quad (3.14a)$$

$$D_S^<(\lambda; t, t') = G_f^<(\lambda; t, t') G_b^>(\lambda; t', t), \quad (3.14b)$$

$$\begin{aligned} D_S^r(\lambda; t, t') = & -G_f^r(\lambda; t, t') G_b^<(\lambda; t', t) \\ & - G_f^<(\lambda; t, t') G_b^a(\lambda; t', t). \end{aligned} \quad (3.14c)$$

After Fourier transform, we get

$$D_S^>(\lambda; \omega) = - \int \frac{d\zeta}{2\pi} G_f^>(\lambda; \omega + \zeta) G_b^<(\lambda; \zeta), \quad (3.15a)$$

$$D_S^<(\lambda; \omega) = \int \frac{d\zeta}{2\pi} G_f^<(\lambda; \omega + \zeta) G_b^>(\lambda; \zeta), \quad (3.15b)$$

$$\begin{aligned} D_S^r(\lambda; \omega) = & - \int \frac{d\zeta}{2\pi} [G_f^r(\lambda; \omega + \zeta) G_b^<(\lambda; \zeta) \\ & + G_f^<(\lambda; \omega + \zeta) G_b^a(\lambda; \zeta)]. \end{aligned} \quad (3.15c)$$

From the projection to the physical Hilbert space $Q=1$ of the Green's function at the dot S , we find the projection rules for the pseudoparticle Green's functions,

$$\begin{aligned} D_S^r(\omega) = & \frac{1}{Z_{S\lambda \rightarrow \infty}} \lim_{\lambda \rightarrow \infty} e^{\beta\lambda} D_S^r(\lambda; \omega) \\ = & - \frac{1}{Z_{S\lambda \rightarrow \infty}} \lim_{\lambda \rightarrow \infty} e^{\beta\lambda} \int \frac{d\zeta}{2\pi} [G_f^r(\lambda; \omega + \zeta + \lambda) G_b^<(\lambda; \zeta + \lambda) \\ & + G_f^<(\lambda; \omega + \zeta + \lambda) G_b^a(\lambda; \zeta + \lambda)] \\ = & - \frac{1}{Z_S} \int \frac{d\zeta}{2\pi} [G_f^r(\omega + \zeta) G_b^<(\zeta) + G_f^<(\omega + \zeta) G_b^a(\zeta)], \end{aligned} \quad (3.16)$$

$$Z_S = \int \frac{d\omega}{2\pi} [N_s G_f^<(\omega) - G_b^<(\omega)]. \quad (3.17)$$

Since the pseudoparticle Green's functions are centered at $\omega = E_S + \lambda$ (pseudofermion) and at $\omega = \lambda$ (slave boson), we have to shift the integration variable before taking the limit

$\lambda \rightarrow \infty$. For $D_S^r(\omega)$ to be well-defined, the limiting pseudoparticle Green's functions should be defined as

$$G_{b,f}^r(\omega) \equiv \lim_{\lambda \rightarrow \infty} G_{b,f}^r(\lambda; \omega + \lambda), \quad (3.18a)$$

$$G_{b,f}^<(\omega) \equiv \lim_{\lambda \rightarrow \infty} e^{\beta\lambda} G_{b,f}^<(\lambda; \omega + \lambda). \quad (3.18b)$$

The second equation means that $\lim_{\lambda \rightarrow \infty} G_{b,f}^<(\lambda; \omega + \lambda) = 0$. Applying the projection procedure to the lesser and greater Green's functions of the dot S , we find the additional projection rules for the pseudoparticle Green's functions:

$$G_{b,f}^>(\omega) \equiv \lim_{\lambda \rightarrow \infty} G_{b,f}^>(\lambda; \omega + \lambda). \quad (3.19)$$

Accordingly, the lesser and greater Green's functions of the dot S are given by the equations

$$D_S^<(\omega) = \frac{1}{Z_S} \int \frac{d\zeta}{2\pi} G_f^<(\omega + \zeta) G_b^>(\zeta), \quad (3.20a)$$

$$D_S^>(\omega) = - \frac{1}{Z_S} \int \frac{d\zeta}{2\pi} G_f^>(\omega + \zeta) G_b^<(\zeta). \quad (3.20b)$$

Applying the projection procedure to the physical Green's function D_S at the dot S , we obtained the projection rules for the pseudoparticle Green's functions.

We are now in a position to find the self-energy equations projected to the physical Hilbert space, $Q=1$, for the pseudoparticle Green's functions,

$$\Sigma_{b,f}^{r,>}(\omega) = \lim_{\lambda \rightarrow \infty} \Sigma_{b,f}^{r,>}(\lambda; \omega + \lambda), \quad (3.21a)$$

$$\Sigma_{b,f}^<(\omega) = \lim_{\lambda \rightarrow \infty} e^{\beta\lambda} \Sigma_{b,f}^<(\lambda; \omega + \lambda). \quad (3.21b)$$

By comparing the self-energies, we can see the identities $G_{b,f}^r(\omega) = G_{b,f}^>(\omega)$,

$$\Sigma_f^<(\omega) = -|W|^2 \int \frac{d\zeta}{2\pi} G_b^<(\omega - \zeta) \tilde{D}_A^<(\zeta), \quad (3.22a)$$

$$\Sigma_f^r(\omega) = |W|^2 \int \frac{d\zeta}{2\pi} G_b^r(\omega - \zeta) \tilde{D}_A^>(\zeta), \quad (3.22b)$$

$$\Sigma_b^<(\omega) = -N_s |W|^2 \int \frac{d\zeta}{2\pi} G_f^<(\omega + \zeta) \tilde{D}_A^>(\zeta), \quad (3.22c)$$

$$\Sigma_b^r(\omega) = N_s |W|^2 \int \frac{d\zeta}{2\pi} G_f^r(\omega + \zeta) \tilde{D}_A^<(\zeta). \quad (3.22d)$$

These are the NCA self-energy equations out of equilibrium. Now inserting the equations

$$\tilde{D}_A^<(\omega) = |\tilde{D}_A^r(\omega)|^2 [2\Gamma_L(\omega) f_L(\omega) + 2\Gamma_R(\omega) f_R(\omega)], \quad (3.23a)$$

$$\bar{D}_A^>(\omega) = |\bar{D}_A^r(\omega)|^2 [2\Gamma_L(\omega)f_L(-\omega) + 2\Gamma_R(\omega)f_R(-\omega)], \quad (3.23b)$$

we find the final version of the NCA equations,

$$\begin{aligned} \Sigma_f^<(\omega) = & - \sum_{p=L,R} \int \frac{d\xi}{\pi} |W|^2 |\bar{D}_A^r(\xi)|^2 \Gamma_p(\xi) f_p(\xi) \\ & \times G_b^<(\omega - \xi), \end{aligned} \quad (3.24a)$$

$$\Sigma_f^r(\omega) = \sum_{p=L,R} \int \frac{d\xi}{\pi} |W|^2 |\bar{D}_A^r(\xi)|^2 \Gamma_p(\xi) f_p(-\xi) G_b^r(\omega - \xi), \quad (3.24b)$$

$$\begin{aligned} \Sigma_b^<(\omega) = & -N_s \sum_{p=L,R} \int \frac{d\xi}{\pi} |W|^2 |\bar{D}_A^r(\xi)|^2 \Gamma_p(\xi) \\ & \times f_p(-\xi) G_f^<(\omega + \xi), \end{aligned} \quad (3.24c)$$

$$\Sigma_b^r(\omega) = N_s \sum_{p=L,R} \int \frac{d\xi}{\pi} |W|^2 |\bar{D}_A^r(\xi)|^2 \Gamma_p(\xi) f_p(\xi) G_f^r(\omega + \xi). \quad (3.24d)$$

The effective Anderson hybridization for a side-connected dot S is given by $\Gamma_{\text{eff}}(\omega) = |W|^2 |\bar{D}_A^r(\omega)|^2 [\Gamma_L(\omega) + \Gamma_R(\omega)]$. Although the dot S is not directly coupled to the external electrodes, it can experience the bias potential difference via the active dot A .

IV. NUMERICAL RESULTS

For the numerical calculations, we assume the constant energy-independent tunneling matrix between the active quantum dot A and two electrodes. The left and right electrodes are assumed to be described by the same Lorentzian density of states (DOS). The self-energies due to the tunneling into the electrodes are found in a closed form in this case. The auxiliary Green's function for the active dot A (\bar{D}_A^r) and the effective Anderson hybridization function for the side-connected dot S [$\Gamma_{\text{eff}}(\omega) = \bar{\Gamma}_L(\omega) + \bar{\Gamma}_R(\omega)$] are given by the equations

$$\bar{D}_A^r(\omega) = \frac{1}{\hbar\omega - E_A - \Gamma \times \frac{D}{\hbar\omega + iD}}, \quad (4.1)$$

$$\bar{\Gamma}_p(\omega) = \Gamma_p |W|^2 \frac{D^2}{[\hbar\omega(\hbar\omega - E_A) - \Gamma D]^2 + (\hbar\omega - E_A)^2 D^2}. \quad (4.2)$$

Here D is the conduction-band width of the Lorentzian DOS. The tunneling rate of an active dot A into the electrodes $\Gamma = \Gamma_L + \Gamma_R$ or the effective bandwidth of Anderson hybridization $\Gamma_{\text{eff}}(\omega)$ will be taken as an energy unit in our numerical works. For this model, the Kondo temperature at zero source-drain bias voltage can be estimated within an order of 1 by the equation

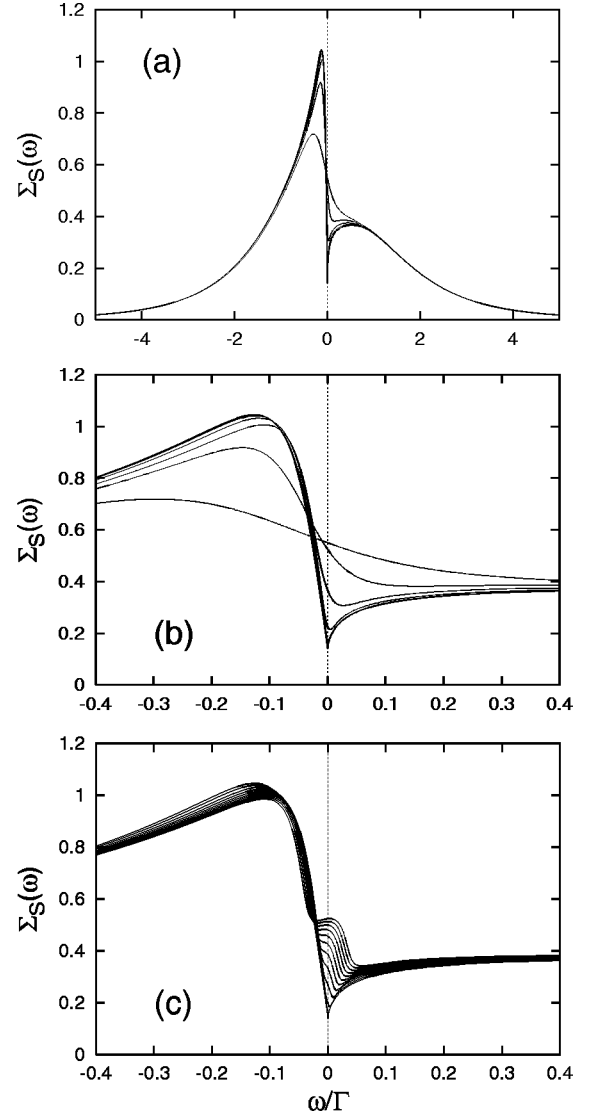


FIG. 3. Temperature and bias voltage dependence of the self-energy of a side-connected dot S . Temperature variation of the self-energy is displayed in (a). The panel (b) is the magnified view of the panel (a) near $\omega=0$. With decreasing temperatures, the structure in the self-energy becomes sharper near $\omega=0$. Temperature variations are $T/T_K = 31.6, 10, 3.16, 1, 3.16 \times 10^{-1}, 10^{-1}, 3.16 \times 10^{-2}, 10^{-2}, 3.16 \times 10^{-3}, 10^{-3}$. At $T = 10^{-3} \times T_K$, the variation of the self-energy with increasing bias voltage is displayed in (c). The source-drain bias voltages are varied from $eV=0$ to $eV=20 \times T_K$ by the amount $2 \times T_K$.

$$T_K = \Gamma \times \exp\left(-\frac{\pi |E_S|}{2\Gamma_{\text{eff}}}\right). \quad (4.3)$$

Here $\Gamma_{\text{eff}} = |W|^2/\Gamma$ is the effective Anderson hybridization at $\omega=0$ and $E_A=0$.

Self-energies. The self-energy Σ_S of a side-connected dot S is obtained from the Green's function D_S , which is calculated from Eq. (3.16), using the relation $\Sigma_S^r = [D_S^r]^{-1} - [D_{S0}^r]^{-1}$. The imaginary part of Σ_S^r is displayed in Fig. 3. Displayed results are corrected to satisfy the causality relation for the Green's function at the active dot A . This correc-

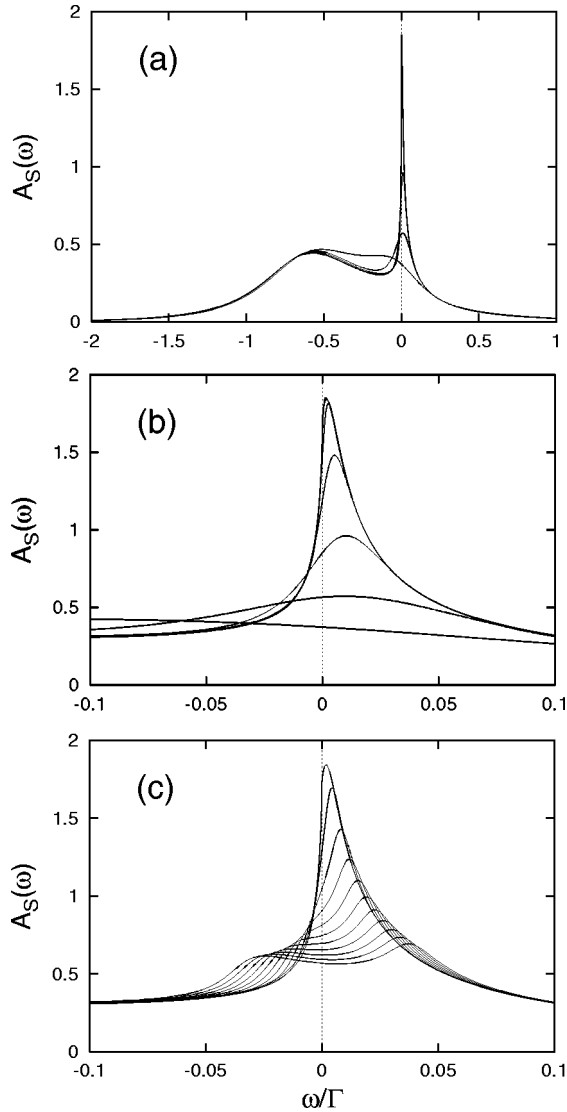


FIG. 4. Temperature and bias voltage dependence of the spectral function $A_S(\omega)$ at a side-connected dot S . (a) and (b) show the developments of a Kondo resonance peak with decreasing temperature. The panel (b) is a magnified view of the panel (a). The bias voltage dependence of the spectral function $A_S(\omega)$ at $T = 10^{-3} \times T_K$ is displayed in (c). The Kondo resonance peak is progressively suppressed with the increasing bias voltage and develops into a two-peak structure. Temperature and voltage variations are the same as in Fig. 3.

tion procedure is explained in Appendix C; see also Ref. 18. With decreasing temperature, a sharp feature develops near $\omega=0$, which is a sign of a Kondo resonance peak. When a finite source-to-drain bias voltage is applied, the sharp structure near $\omega=0$ becomes smooth and splits into two at $\omega = \pm eV/2$.

Spectral functions. The spectral functions are calculated from the imaginary part of the Green's functions,

$$A_i(\omega) = -\frac{1}{\pi} \text{Im} D_i^r(\omega), \quad i=A,S, \quad (4.4)$$

and displayed in Figs. 4 and 5. The spectral function $A_S(\omega)$

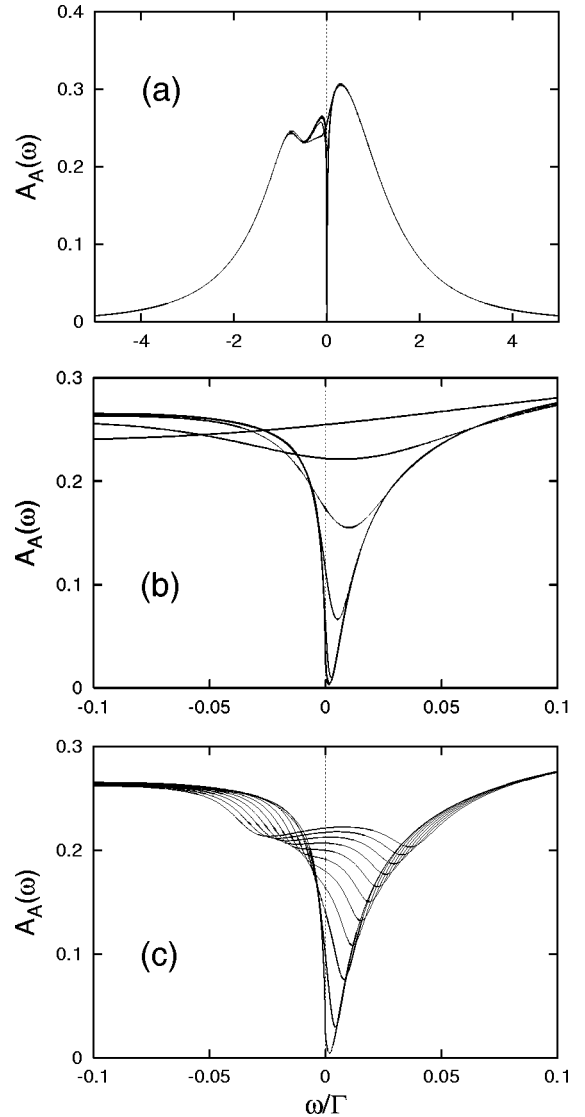


FIG. 5. Temperature and bias voltage dependence of the spectral function $A_A(\omega)$ at the active dot A . Due to the Fano interference, the spectral function $A_A(\omega)$ becomes depleted near $\omega=0$ as the temperature is lowered below T_K , as shown in (a) and (b). When a finite bias voltage is applied, the spectral depletion is refilled and the two-peak structure in $A_S(\omega)$ is manifested as the double-dip structure in $A_A(\omega)$. Temperature and voltage variations are the same as in Fig. 3.

at a side-connected dot S develops the Kondo resonance peak near $\omega=0$ with decreasing temperature below $T < T_K$. The Green's function at the active dot A is renormalized according to Eq. (2.22). As the side-connected dot S develops the Kondo resonance, the spectral function $A_A(\omega)$ at the active dot A is depleted near $\omega=0$. The spectral depletion can be understood as the destructive interference between the direct path and the indirect path (Fano interference). The spectral depletion leads to the suppression of the current flowing through the dot A . The width of the depleted region is given by the Kondo temperature (4.3) of the dot S . When a finite value of source-to-drain bias voltage is applied, the peak in $A_S(\omega)$ and the dip in $A_A(\omega)$ near $\omega=0$ split into two at

$= \pm eV/2$. The two Kondo resonance peaks in $A_S(\omega)$ and dips in $A_A(\omega)$ become pinned at the Fermi energies of the left and right electrodes.^{16,17}

Since the NCA underestimates the one-body contribution of the self-energy Σ_S (side-connected dot) from tunneling into the effective continuum band, our NCA calculation of the spectral function at the active dot A shows negative spectral weight near the depleted region (violation of the causality relation). This is purely an artifact of the NCA. Since the NCA is based on the expansion in powers of the Anderson hybridization (in our case W) and includes only a subset of diagrams up to infinite order in W without vertex corrections, the underestimation is expected. Though the NCA underestimates the one-body contribution of the self-energy, its dependence on the energy and temperature turns out to be correct close to $\omega=0$ and at $T>0$ K. The NCA leads to pathological results at and near $T=0$ K.¹⁴ From the Fermi-liquid relation, it can be shown that the spectral function of the active dot A is zero at $\omega=0$ at zero temperature. According to the Fermi-liquid theory, the magnetic ion's spectral function [$A_S(\omega)$ in our case] can be related to the phase shift of conduction electrons (electrons at the active dot A in our case) at the Fermi energy. The phase shift is determined by the Langreth-Friedel sum rule,¹⁹ $n_S = 2(\delta/\pi)$, where the numerical factor 2 accounts for two possible spin directions,

$$A_S(0) = \frac{1}{\pi\Gamma_{\text{eff}}} \sin^2 \frac{\pi n_S}{2}, \quad (4.5)$$

where $\Gamma_{\text{eff}} = |W|^2/\Gamma$ is the effective Anderson hybridization for a side-connected dot S at $\omega=0$. With complete screening, n_S is equal to 1. Inserting the Fermi-liquid relation into Eq. (2.22), it can be shown that the spectral function of the active dot A vanishes at $\omega=0$, or $A_A(0)=0$.

To compensate for the NCA's underestimation of the self-energy, we corrected the self-energy by adding a term proportional to one-body self-energy $|W|^2 \bar{D}_A^r(\omega)$ to it such that the spectral function A_A of the active dot remains non-negative definite and $A_A(0) \rightarrow 0$ with the temperature approaching zero. Since the contribution to the self-energy coming from the hybridization with the effective continuum band is of one-body nature and temperature-independent, this correction procedure is not a bad idea.

Linear-response conductance. The linear-response conductance $\sigma(T)$ is calculated by differentiating Eq. (2.21a) with respect to the source-drain bias voltage at $V=0$,

$$\sigma(T) = \frac{2e^2}{h} \int d\epsilon T(\epsilon) \left[-\frac{\partial f(\epsilon)}{\partial \epsilon} \right]. \quad (4.6)$$

As shown in Fig. 6, $\sigma(T)$ is suppressed with decreasing temperature. The conductance shows a logarithmic dependence on temperature near the Kondo temperature. From Fermi-liquid theory, it can be expected that the conductance is completely suppressed at zero temperature. The electron flow is blocked by the destructive interference between two different paths: the direct path ($L \rightarrow A \rightarrow R$) and the indirect one ($L \rightarrow A \rightarrow S \rightarrow A \rightarrow R$).

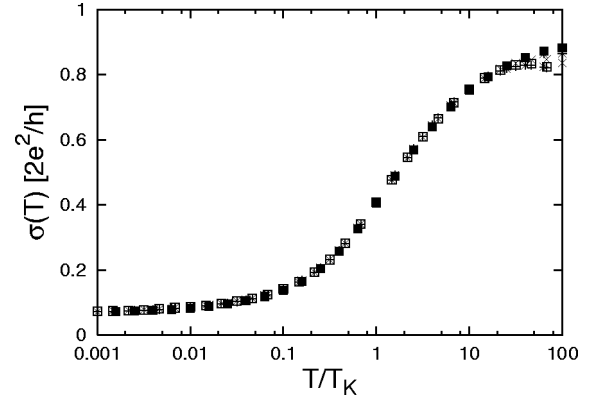


FIG. 6. Temperature dependence of linear-response conductance $\sigma(T)$. The conductance at $V=0$ is suppressed with decreasing temperature as can be expected from the temperature dependence of the spectral function $A_A(\omega)$. The conductance is suppressed logarithmically due to the enhanced Kondo scattering near the Kondo temperature and becomes saturated with decreasing temperature. $\sigma(T)$ shows the scaling behavior over a wide range of temperature. Symbols mean different sets of model parameters or differing Kondo temperatures.

This suppressed behavior of $\sigma(T)$ at low temperatures is another example of zero-bias anomalies (ZBA's) observed in several mesoscopic devices. Scattering of conduction electrons off the Kondo impurities is one of the scenarios explaining ZBA's. Depending on the topology of mesoscopic devices and Kondo impurities, the ZBA can lead to the enhanced or suppressed conductance at low temperature.

As expected from the Kondo effect, the linear-response conductance $\sigma(T)$ shows the scaling behavior over a wide range of temperature. Several curves of $\sigma(T)$ for different sets of model parameters (differing Kondo temperature) collapse onto one curve as shown in Fig. 6.

Differential conductance. The current flowing from the left to right electrode is calculated using Eq. (2.21a). Differential conductance $G(T, V) = dI/dV$ is obtained by differentiating the current with respect to a finite source-drain bias voltage. Differential conductance is displayed in Fig. 7. With decreasing temperature, dI/dV is suppressed near zero source-drain bias voltage. The pseudogap behavior of the spectral function at the active quantum dot A explains this I - V characteristic.

V. CONCLUSION

In this work, we studied the transport properties of parallel double quantum dots when only the *active* dot is coupled to the two external electrodes and the other dot is *side-connected* to the active dot. When the active dot lies in the conductance peak region and the side-connected dot in the Coulomb-blockade region, the current flow through the active dot is suppressed due to the Kondo scattering off the effective spin in the side-connected dot. Suppressed conductance at low temperature and near zero bias voltage can be understood in terms of Fano interference between two paths: direct path of left electrode–active dot–right electrode and indirect path of left electrode–active dot–side-connected

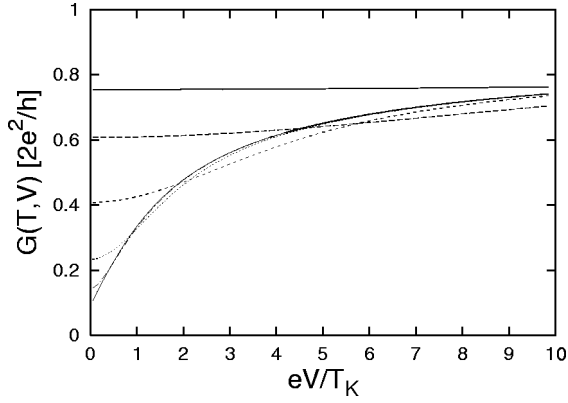


FIG. 7. Differential conductance $G(T, V) = dI/dV$ with varying temperature. The differential conductance is progressively suppressed near zero bias voltage with lowering temperature. From top, the temperature variations are $T/T_K = 10, 3.16, 1, 3.16 \times 10^{-1}, 10^{-1}, 3.16 \times 10^{-2}, 10^{-2}, 10^{-3}$. The last three curves cannot be distinguished with the naked eye.

dot–active dot–right electrode. Our study suggests the possibility that the current flowing through one quantum dot can be controlled experimentally by an additional side-connected quantum dot.

ACKNOWLEDGMENTS

This work is supported in part by the BK21 project and in part by the National Science Foundation under Grant No. DMR 9357474.

APPENDIX A: NONINTERACTING CASE: $U_A = U_S = 0$

When $U_A = U_S = 0$, both active and side-connected dots become resonant levels. The current and its noise can be obtained analytically in a closed form. The self-energies of the dots A and S are

$$\Sigma_A(t, t') = \Sigma_c(t, t') + |W|^2 D_{S0}(t, t'), \quad (\text{A1})$$

$$\Sigma_S(t, t') = |W|^2 \tilde{D}_A(t, t'). \quad (\text{A2})$$

Here the one-body self-energy Σ_c is given by the equation

$$\Sigma_c(t, t') = \frac{1}{V} \sum_{pk} |V_p(\vec{k})|^2 G_{cp}(\vec{k}; t, t'),$$

and the auxiliary Green's functions \tilde{D}_A and \tilde{D}_S are given by the equations

$$\begin{aligned} \tilde{D}_A(t, t') &= D_{A0}(t, t') + \int_C dt_1 \int_C dt_2 \tilde{D}_A(t, t_1) \\ &\quad \times \Sigma_c(t_1, t_2) D_{A0}(t_2, t'), \end{aligned} \quad (\text{A3})$$

$$\tilde{D}_S(t, t') = D_{S0}(t, t'). \quad (\text{A4})$$

The self-energy of the auxiliary Green's function \tilde{D}_A is given by $\tilde{\Sigma}_A(t, t') = \Sigma_c(t, t')$.

The retarded Green's functions can be readily obtained,

$$D_A^r(\omega) = \frac{\hbar\omega - E_S}{[\hbar\omega - E_S] \times [\hbar\omega - E_A - \Sigma_c^r(\omega)] - |W|^2}, \quad (\text{A5})$$

$$D_S^r(\omega) = \frac{\hbar\omega - E_A - \Sigma_c^r(\omega)}{[\hbar\omega - E_S] \times [\hbar\omega - E_A - \Sigma_c^r(\omega)] - |W|^2}. \quad (\text{A6})$$

Due to the Fano interference, the spectral function of the active dot A vanishes at $\omega = E_S$. On the other hand, the spectral function of the side-connected dot S is peaked at $\omega = E_S$. The nonequilibrium distribution function of the dot S is also readily calculated,

$$\begin{aligned} \tilde{\Sigma}_A^<(\omega) &= 2\Gamma_L(\omega)f_L(\omega) + 2\Gamma_R(\omega)f_R(\omega), \\ -\text{Im} \tilde{\Sigma}_A^r(\omega) &= \Gamma_L(\omega) + \Gamma_R(\omega), \end{aligned} \quad (\text{A7})$$

$$f_{\text{eff}}(\omega) = \frac{\tilde{\Sigma}_A^<(\omega)}{-2\text{Im} \tilde{\Sigma}_A^r(\omega)} = \frac{\Gamma_L(\omega)f_L(\omega) + \Gamma_R(\omega)f_R(\omega)}{\Gamma_L(\omega) + \Gamma_R(\omega)}.$$

The full self-energies of the active dot A are

$$\begin{aligned} \Sigma_A^<(\omega) &= 2\Gamma_L(\omega)f_L(\omega) + 2\Gamma_R(\omega)f_R(\omega) + |W|^2 \tilde{D}_S^<(\omega), \\ \Sigma_A^r(\omega) - \Sigma_A^a(\omega) &= -2i[\Gamma_L(\omega) + \Gamma_R(\omega)] \\ &\quad + |W|^2[\tilde{D}_S^r(\omega) - \tilde{D}_S^a(\omega)]. \end{aligned} \quad (\text{A8})$$

To determine $\tilde{D}_S^<(\omega)$, we use the condition $I_S = 0$ (the number of electrons in the dot S remains the same),

$$\tilde{D}_S^<(\omega) = 2\pi \frac{\Gamma_L(\omega)f_L(\omega) + \Gamma_R(\omega)f_R(\omega)}{\Gamma_L(\omega) + \Gamma_R(\omega)} \tilde{A}_S(\omega). \quad (\text{A9})$$

Here $\tilde{A}_S(\omega) = \delta(\hbar\omega - E_S)$.

Inserting all the equations into the expression of the current (2.7), we find the current flowing from the left electrode to the right one,

$$\begin{aligned} I_L &= e \sum_{\alpha} \int \frac{d\omega}{2\pi} \{ 4\Gamma_L(\omega)\Gamma_R(\omega) |D_A^r(\omega)|^2 [f_R(\omega) - f_L(\omega)] \\ &\quad + 2|W|^2 \Gamma_L(\omega) |D_A^r(\omega)|^2 [\tilde{D}_S^<(\omega) - 2\pi f_L(\omega) \tilde{A}_S(\omega)] \} \\ &= \frac{e}{h} \sum_{\alpha} \int d\epsilon T(\epsilon) [f_R(\epsilon) - f_L(\epsilon)]. \end{aligned} \quad (\text{A10})$$

The transmission spectral function $T(\epsilon)$ is given by the equation

$$\begin{aligned} T(\epsilon) &= 4\Gamma_L(\epsilon)\Gamma_R(\epsilon) |D_A^r(\epsilon)|^2 \left[1 + \frac{\pi |W|^2 \tilde{A}_S(\epsilon)}{\Gamma_L(\epsilon) + \Gamma_R(\epsilon)} \right] \\ &= \frac{4\pi\Gamma_L(\epsilon)\Gamma_R(\epsilon)}{\Gamma_L(\epsilon) + \Gamma_R(\epsilon)} A_A(\epsilon). \end{aligned} \quad (\text{A11})$$

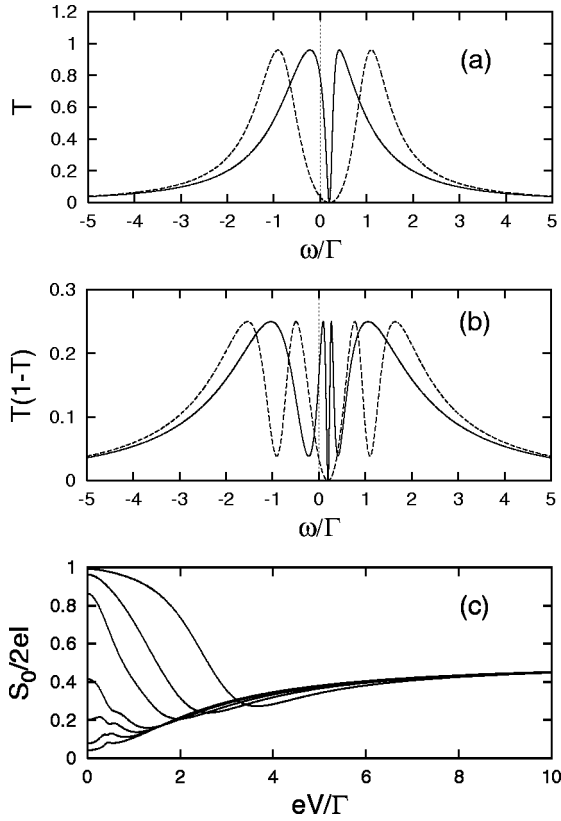


FIG. 8. Tunneling coefficients and Fano factor at $T=0$ K. Due to the Fano interference, the transmission coefficient $T(\omega)$ is completely suppressed when $\omega=E_S$, the energy level of the side-connected dot. The Fano factor, $F=S_0/2eI$, has a dip structure accordingly. The model parameters are $E_A=0$, $E_S/\Gamma=0.2$ for displayed curves. In (a) and (b), $W/\Gamma=0.3$ (1.0) for solid (dashed) line, respectively. In panel (c), the values of W/Γ are varied from the bottom successively as 0.1,0.2,0.3,0.4,0.7,1.0,1.5.

The current noise, defined as the current-current correlation function, can be obtained in a closed form in the noninteracting case,

$$S(t,t')=\langle\delta I(t)\delta I(t')\rangle+\langle\delta I(t')\delta I(t)\rangle. \quad (\text{A12})$$

Here $\delta I=I-\langle I\rangle$. Defining the current Green's function by

$$i\hbar G_{II}(t,t')=\langle T\delta I(t)\delta I(t')\rangle, \quad (\text{A13})$$

the current-current correlation function can be written as $S(t,t')=\hbar G_{II}^>(t,t')+\hbar G_{II}^<(t',t)$. Six diagrams are contributing to the current noise and the static current noise $S_0=S(\omega=0)$ is given by the well-known formula²⁰

$$S_0=\frac{4e^2}{h}\int d\epsilon T(\epsilon)\{f_L(\epsilon)[1-f_L(\epsilon)]+f_R(\epsilon)[1-f_R(\epsilon)]\} \\ +\frac{4e^2}{h}\int d\epsilon T(\epsilon)[1-T(\epsilon)]\{f_L(\epsilon)-f_R(\epsilon)\}^2. \quad (\text{A14})$$

The first line is the thermal Johnson noise and the second line is called the shot noise coming from a finite source-drain bias voltage.

Typical results at $T=0$ K are displayed in Fig. 8 for the

transmission coefficient $T(\epsilon)$ and the Fano factor $F=S_0/2eI$. Due to the Fano interference, the transmission coefficient is completely suppressed at $\omega=E_S$, the energy level of the side-connected dot. This structure leads to a dip in the Fano factor. The Fano factor F takes the following values at $V=0$ and $V\rightarrow\infty$:

$$F(V=0)=1-\frac{4\Gamma_L\Gamma_R}{(\Gamma_L+\Gamma_R)^2}\frac{E_S^2}{E_S^2+(E_A E_S-W)^2/\Gamma^2},$$

$$F(V\rightarrow\infty)=1-\frac{2\Gamma_L\Gamma_R}{(\Gamma_L+\Gamma_R)^2}.$$

Here $\Gamma=\Gamma_L+\Gamma_R$. The limiting value of F at $eV\gg\Gamma$ is solely determined by the tunneling rates, Γ_L and Γ_R .

APPENDIX B: INTERACTING CASE: $U_A\neq 0$ AND $U_S\neq 0$

When both dots A and S are strongly correlated, the model system becomes highly nontrivial due to many-body effects. In this section, we derive the effective spin exchange interaction when both dots lie in the Kondo limit or in the absence of charge fluctuations. Our model space \mathcal{M} and its orthogonal space $\bar{\mathcal{M}}$ are then given by

$$\mathcal{M}=|A\alpha\rangle\otimes|S\beta\rangle=|A\alpha;S\beta\rangle, \quad \alpha,\beta=\uparrow,\downarrow, \quad (\text{B1})$$

$$\bar{\mathcal{M}}=|A\alpha;S\rho\rangle, \quad |A\rho;S\alpha\rangle, \quad |A\rho;S\rho'\rangle,$$

$$\alpha,\beta=\uparrow,\downarrow; \quad \rho,\rho'=\pm. \quad (\text{B2})$$

Here α and β represent the spin-up or -down state, while ρ and ρ' are the isospin state:

$$|i+\rangle=d_{i\uparrow}^\dagger d_{i\downarrow}^\dagger|0\rangle, |i-\rangle=|0\rangle, i=A,S,$$

where $|0\rangle$ means the empty state of a quantum dot.

To find the effective spin-exchange Hamiltonian, we need to evaluate the following matrix elements:

$$\langle A\alpha;S\beta|H_1|A\mu;S\rho\rangle=0,$$

$$\langle A\alpha;S\beta|H_1|A\rho;S\mu\rangle$$

$$=\delta_{\beta,\mu}\langle A\alpha|H_1|A\rho\rangle$$

$$=\delta_{\beta,\mu}\times\left\{\sum_{pk}V_p^*(\vec{k})c_{p\vec{k}\alpha}c_{\rho,-}\right.$$

$$\left.+(-1)^{\alpha-1/2}\sum_{pk}V_p(\vec{k})c_{p\vec{k}\alpha}^\dagger c_{\rho,+}\right\},$$

$$\langle A\alpha;S\beta|H_1|A\rho;S\rho'\rangle=(-1)^{\alpha-1/2}W\delta_{\alpha+\beta,0}\delta_{\rho+\rho',0}.$$

When the charge fluctuations can be neglected, we find the effective spin-exchange Hamiltonian

$$\bar{H}_1=\sum_{p\vec{k}\alpha}\sum_{p'\vec{k}'\beta}J_{pp'}(\vec{k},\vec{k}')c_{p\vec{k}\alpha}^\dagger\frac{1}{2}\vec{\sigma}_{\alpha\beta}c_{p'\vec{k}'\beta}\cdot\vec{S}_A \\ +J_{AS}(\vec{S}_A\cdot\vec{S}_S-\frac{1}{4}), \quad (\text{B3})$$

$$J_{pp'}(\vec{k}, \vec{k}') = 2V_p(\vec{k})V_{p'}^*(\vec{k}') \left[\frac{1}{-E_A} + \frac{1}{E_A + U_A} \right], \quad (\text{B4})$$

$$J_D = 2|W|^2 \left[\frac{1}{E_A + U_A - E_S} + \frac{1}{E_S + U_S - E_A} \right]. \quad (\text{B5})$$

Electrons are scattered off an effective spin \vec{S}_A at the active dot and can flow from one electrode to the other. Since \vec{S}_A is coupled antiferromagnetically to \vec{S}_S , the occurrence of enhanced Kondo scattering at low temperature depends on the magnitude of antiferromagnetic coupling J_{AS} relative to, e.g., the Kondo temperature. When $J_{AS} \gg T_K$, a spin-singlet formation between two dots is favored over the many-body Kondo singlet state and the enhanced Kondo scattering is not expected. On the other hand, when $T_K \gg J_{AS}$, a Kondo singlet state is expected to be favored over a spin-singlet state between two dots and the conductance will be enhanced due to the Kondo scattering at low temperature. Detailed study of this model in equilibrium is in progress using Wilson's numerical renormalization group method and will be published elsewhere.

APPENDIX C: FERMI-LIQUID RELATIONS

In this section, we discuss the correction of pathological behavior of NCA near $\omega=0$. The Green's function of the dot A is related to that at the dot S by Eq. (2.22). The causality is seldom violated when the number of channels is

larger than two. On the other hand, the causality is violated for the case of one channel near $\omega=0$ at temperatures below the Kondo temperature T_K . The recently developed conserving t -matrix approximation (CTMA) (Ref. 21) may have a chance to overcome this pathology. In this paper, we are going to remedy this pathology of the NCA by *adding* a one-body self-energy correction to the self-energy $\Sigma_S(\omega)$ to satisfy the Fermi-liquid relation. The self-energy for the dot S can be written as a sum of two contributions,

$$\Sigma_S^r(\omega) = \Sigma_{\text{hyb}}^r(\omega) + \Sigma_U^r(\omega), \quad \Sigma_{\text{hyb}}^r(\omega) = |W|^2 \tilde{D}^r(\omega). \quad (\text{C1})$$

The self-energy $\Sigma_{\text{NCA}}^r(\omega)$ calculated from the NCA is known to show the correct energy and temperature dependence near $\omega=0$ and $T=0$. (Temperature must be higher than the pathological temperature estimated in, e.g., Ref. 14.) We assume that $\Sigma_U^r(\omega)$ is well-captured in the NCA. Since $-\text{Im} \Sigma_U^r(\omega) \propto \omega^2 + [\pi k_B T]^2$ for $\omega, T < T_K$ (see Ref. 22), we add the correction term to Σ_{NCA}^r in order to make $D_A^r(\omega)$ obey the causality relation,¹⁸

$$\Sigma_S^r(\omega) \approx \Sigma_{\text{NCA}}^r(\omega) + (|W|^2 - W_{\text{NCA}}^2) \tilde{D}_A^r(\omega). \quad (\text{C2})$$

Here W_{NCA}^2 is determined numerically from the calculated $\Sigma_{\text{NCA}}^r(\omega)$ at the lowest possible temperature,

$$\frac{W_{\text{NCA}}^2}{\Gamma} \equiv -\text{Im} \Sigma_{\text{NCA}}^r(0). \quad (\text{C3})$$

-
- ¹L. I. Glazman and M. E. Raikh, JETP Lett. **47**, 452 (1988); T. K. Ng and P. A. Lee, Phys. Rev. Lett. **61**, 1768 (1988).
²D. Goldhaber-Gordon, H. Shtrikman, D. Malahu, D. Abusch-Magder, U. Meirav, and M. A. Kastner, Nature (London) **391**, 156 (1998).
³S. M. Cronenwett, T. H. Oosterkamp, and L. P. Kouwenhoven, Science **281**, 540 (1998).
⁴J. Nygard, D. H. Cobden, and P. E. Lindelof, Nature (London) **408**, 342 (2000).
⁵M. Büttiker and C. A. Stafford, Phys. Rev. Lett. **76**, 495 (1996); V. Ferrari *et al.*, *ibid.* **82**, 5088 (1999).
⁶U. Gerland, J. von Delft, T. A. Costi, and Y. Oreg, Phys. Rev. Lett. **84**, 3710 (2000).
⁷W. G. van der Wiel, S. De Franceschi, T. Fujisawa, J. M. Elzerman, S. Tarucha, and L. P. Kouwenhoven, Science **289**, 2105 (2000).
⁸R. Aguado and D. C. Langreth, Phys. Rev. Lett. **85**, 1946 (2000); C. A. Büsser, E. V. Anda, A. L. Lima, M. A. Davidovich, and G. Chiappe, Phys. Rev. B **62**, 9907 (2000); W. Izumida and O. Sakai, *ibid.* **62**, 10 260 (2000).
⁹S. Sasaki, S. De Franceschi, J. M. Elzerman, W. G. van der Wiel, M. Eto, S. Tarucha, and L. P. Kouwenhoven, Nature (London) **405**, 764 (2000).
¹⁰M. Eto and Yu. V. Nazarov, Phys. Rev. Lett. **85**, 1306 (2000); M. Pustilnik and L. I. Glazman, *ibid.* **85**, 2993 (2000).
¹¹J. R. Schrieffer and P. A. Wolff, Phys. Rev. **149**, 491 (1966).
¹²L. V. Keldysh, Zh. Éksp. Teor. Fiz. **47**, 1515 (1964) [Sov. Phys. JETP **20**, 1018 (1965)]; Y. Meir and N. S. Wingreen, Phys. Rev. Lett. **68**, 2512 (1992).
¹³D. C. Langreth, in *Linear and Nonlinear Electron Transport in Solids*, Vol. 17 of *NATO Advanced Study Institute, Series B: Physics*, edited by J. T. Devreese and V. E. van Doren (Plenum, New York, 1976), p. 3.
¹⁴N. E. Bickers, Rev. Mod. Phys. **59**, 845 (1987); N. E. Bickers, D. L. Cox, and J. W. Wilkins, Phys. Rev. B **36**, 2036 (1987).
¹⁵T.-S. Kim and D. L. Cox, Phys. Rev. B **55**, 12 594 (1997).
¹⁶Y. Meir, N. S. Wingreen, and P. A. Lee, Phys. Rev. Lett. **70**, 2601 (1993); N. S. Wingreen and Y. Meir, Phys. Rev. B **49**, 11 040 (1994).
¹⁷M. H. Hettler, J. Kroha, and S. Hershfield, Phys. Rev. Lett. **73**, 1967 (1994).
¹⁸D. L. Cox and N. Grewe, Z. Phys. B: Condens. Matter **71**, 321 (1988); E. Kim and D. L. Cox, Phys. Rev. B **58**, 3313 (1998).
¹⁹D. C. Langreth, Phys. Rev. **150**, 516 (1966).
²⁰For instance, look at the review article by Ya. M. Blanter and M. Büttiker, Phys. Rep. **336**, 1 (2000).
²¹J. Kroha, P. Wölfe, and T. A. Costi, Phys. Rev. Lett. **79**, 261 (1997).
²²K. Yamada, Prog. Theor. Phys. **53**, 970 (1975); **54**, 316 (1975).